EVOLUTIONARY-BASED PREDICTION OF ε_{50} FOR THE LATERAL LOAD-DISPLACEMENT BEHAVIOR OF PILES IN CLAY

BABAK EBRAHIMIAN and AIDA NAZARI

about the authors

corresponding author

Babak Ebrahimian
University of Tehran,
School of Civil Engineering
Tehran, Iran
E-mail: bebrahimian@ut.ac.ir
The Highest Prestigious Scientific and Professional National Foundation,
Iran's National Elites Foundation (INEF),
Tehran, Iran

Aida Nazari
Iran University of Science and Technology
School of Civil Engineering
Tehran, Iran

Abstract

Analyzing piles that are subjected to lateral loads reveals that their behavior depends on the soil's resistance at any point along the pile as a function of the pile's deflection, known as the p-y curve. On the other hand, the deformation characteristics of soil defined as "the soil strain at 50% of maximum deviatoric stress (ε_{50})" have a considerable effect on the generated p-y curve. In this research, several models are proposed to predict ε_{50} specifically for designing the very long pile foundations of offshore oil and gas platforms in the South Pars field, Persian Gulf, Iran. Herein, ε_{50} is evaluated using extensive soil data, including in-situ and laboratory test results using evolutionary polynomial regression (EPR). The effects of the undrained shear strength, the normalized tip resistance of the cone penetration test, the over-burden pressure, the plasticity index and the over-consolidation ratio on ε_{50} are investigated in marine clays. It is demonstrated that the normalized cone tip resistance, which is an indication of the soil's undrained shear strength, leads to more realistic ε_{50} values compared with the laboratory-derived undrained shear strength parameter. In addition, the application of the soil-index properties and the over-burden pressure in the models, improves their estimation quality. Furthermore, the results of full-scale lateral pile load tests at different sites are used in order to validate the performance of the proposed models when it comes to predicting the behavior of the lateral piles.

keywords

p-y curve; laterally loaded pile; piezocone penetration test (PCPT); marine clay; evolutionary polynomial regression (EPR); South Pars field

1 INTRODUCTION

Pile foundations are often required to be designed against significant lateral, in addition to vertical, loads. These lateral loads can be imposed by wind, earth pressure, wave, tide, current and ship impact, mooring rope, earthquake, vehicle traction, etc. The performance of pile foundations is usually governed by either deflection or bearing capacity. Exceeding the maximum allowable lateral load may cause the failure of the soil around the pile, or structural failure of the pile itself. In order to design a pile foundation safely and economically, an accurate assessment of its behavior should be made using pile load test data and/or the well-known analytical or numerical methods. As full-scale load tests are very expensive and time consuming, analytical and numerical approaches are normally used to evaluate the lateral behavior of pile-soil systems.

The lateral pile-soil interaction behavior is commonly characterized by a series of uncoupled, nonlinear springs applied along the pile, known as p-y curves. Various formulations have been proposed to predict these p-y curves in different site conditions [1-7]. The American Petroleum Institute (API) method [7] is a widely used method based on Matlock's field research [1].

The pile geometry and the soil properties are the key parameters for developing p-y curves. These curves mostly depend on the ultimate horizontal soil reaction (P_u) and the critical lateral displacement (y_c) corresponding to 50% mobilized P_u . y_c is defined as

$$y_c = 2.5\varepsilon_{50}D \qquad (1)$$

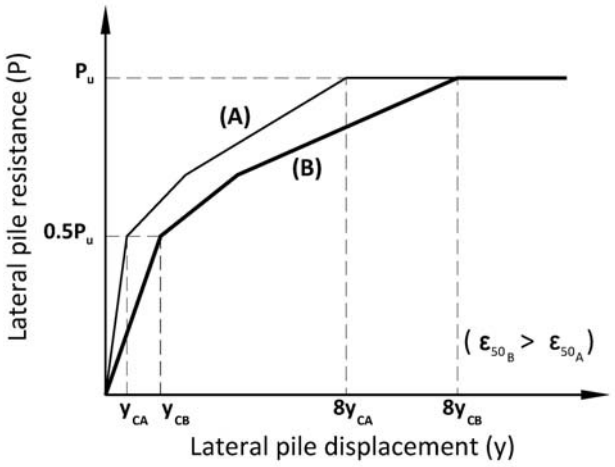

Figure 1. Typical p-y curves for pile in cohesive soil under static loading.

where D is the pile diameter, and ε_{50} is the strain at one-half of the maximum stress in laboratory undrained compression tests on undisturbed cohesive soil samples. Typical p-y curves for cohesive soils, shown in Fig.1, illustrate the role of the above-mentioned parameters on developing such curves. The curves A and B in this figure are schematic p-y curves for soils with different ε_{50} values. As $\varepsilon_{50_B} > \varepsilon_{50_A}$, with the same pile geometry we have $y_{C_B} > y_{C_A}$. As shown in this figure, ε_{50} is an effective factor in generating the p-y curves for clays. It is clear that higher ε_{50} values lead to softer pile behavior and higher lateral displacements for constant lateral load ratios (P/P_u). Furthermore, the ultimate lateral load is obtained at higher levels of pile lateral displacements as the ε_{50} increases. Hence, the lateral stiffness and the resistance of the pile-soil system are affected by ε_{50}.

Sullivan et al. [8] recommended ε_{50} values for different clayey soils based on their undrained shear strength. However, such proposed ε_{50} values are not consistent with those obtained from experimental measurements conducted at different sites and do not result in accurate p-y curves in most soil conditions [9,10].

Hamilton et al. [10] performed some triaxial compression tests under isotropically consolidated undrained (CIU) and unconsolidated undrained (UU) conditions on Tilbrook Grange clays and measured the ε_{50} values. They realized that the ε_{50} values obtained from the CIU tests show less scatter than those of the UU tests and found a trend line for ε_{50}. It was demonstrated that the ε_{50} values obtained from laboratory tests were nearly five times greater than the values recommended by Sullivan for sites having similar undrained shear strengths.

Afterwards, they compared different p-y curves derived from laboratory ε_{50} values and those recommended by Sullivan. It was demonstrated that the uncertainty of the predicted p-y curves decreases from 65% to 35% if the laboratory ε_{50} values are used instead of those recommended by Sullivan. Additionally, they noted that the use of p-y curves based on the Matlock method with ε_{50} values from CIU tests leads to a more reliable prediction of the lateral load-displacement response.

Hamilton et al. [10] discussed different methods to develop p-y curves for piles in stiff, over-consolidated clays. They compared the measured values of ε_{50} derived from UU tests with those typically assumed from the Sullivan recommendations and indicated that a slightly better prediction of the load–displacement curves is achieved using measured ε_{50} values instead of those recommended by Sullivan.

Dunnavant [11] performed experimental and analytical investigations to predict the influences of the pile and soil characteristics as well as the loading conditions on the lateral pile-soil interaction in saturated over-consolidated clays. It was shown that the over-consolidation ratio (OCR) of the soil can affect the reference critical displacement (y_c) in the p-y curves. In other words, for over-consolidated clays, the value of y_c would be smaller than those available in the literature. The degradation of p-y curves in over-consolidated clays begins at much smaller deflections than in soft clays. Also, it was recognized that the pile stiffness and the pile diameter could affect y_c.

Davies [12] and Robertson et al. [6] presented a preliminary semi-empirical method to evaluate p-y curves based on flat dilatometer test (DMT) data. They employed the DMT-based p-y curves to model the behavior of three full-scale lateral pile load tests. They showed that ε_{50} has an increasing trend versus depth in both clays and sands in the considered sites. It was found that the predicted deflections using the DMT results agree well with those obtained from the pile load tests. In all the studied cases the calculated bending moments from the DMT-derived p-y curves were larger than those calculated from the measured pile deflection profiles.

Soil properties such as ε_{50} are very sensitive to soil disturbance due to the coring procedure, and using ε_{50} values based on the tests on core samples may finally lead to a considerable deviation in predicting the real pile behavior. On the other hand, in-situ testing methods, such as the flat dilatometer (DMT), the pressuremeter (PMT) and the cone penetration test (CPT) offer excellent means by which representative soil properties can be obtained [6,12,13]. Therefore, such in-situ tests,

with a minimum soil disturbance, can be used for evaluating ε_{50} and developing p-y curves.

The cone penetration test (CPT) is a reliable in-situ test for its continuous sounding capability and good repeatability. It provides valuable geotechnical information in the soil. Furthermore, the similarity between the CPT penetration process and the pile installation has led to its popularity in deep foundation analysis and design. The total cone tip resistance obtained from the CPT has a strong correlation with the soil's shear strength [14]; on the other hand, due to the direct dependence of ε_{50} on the shear strength, the total tip resistance of the CPT can be employed in evaluating ε_{50} .

Despite the significant influence of ε_{50} on determining the p-y curves, prediction methods used to evaluate this parameter are very rare in the literature. Therefore, this study investigates the use of CPT data to predict ε_{50} in clayey soils and examines the capability of predicted ε_{50} values to generate realistic p-y curves for laterally loaded piles at different sites. The present calculations of ε_{50} are based on a comprehensive databank from laboratory and field tests, performed in the South Pars field, Persian Gulf, southwest of Iran. The field is an extremely strategic offshore area which contains the world's largest gas resources. Many gas-extraction facilities supported on long pile foundations have been constructed in this important region and a large number of such facilities are still under development. Hence, this research mainly focuses on an accurate evaluation of ε_{50} as an influential parameter in the analysis and design of piles against lateral loads in this region. In this regard, several statistical models based on the evolutionary polynomial regression (EPR) method are proposed to evaluate the ε_{50} values for clayey soils. The effects of the cone tip resistance, the undrained shear strength, the over-burden pressure as well as different index properties of the soils, such as the over-consolidation ratio and the plasticity index on ε_{50} are evaluated and discussed. In particular, the effect of the undrained shear strength of the cohesive soils obtained from field tests on ε_{50} is investigated and compared with the recommended values available in the literature. Finally, the validation of the proposed models is performed for full-scale piles tested at two different sites with different soil conditions.

2 SITE DESCRIPTION

The survey area, approximately 50×45 km^2, is located in the Persian Gulf, Iran, between 27° 27' to 27° 28' Northing and 52° 27' to 52° 44' Easting (Fig. 2). The

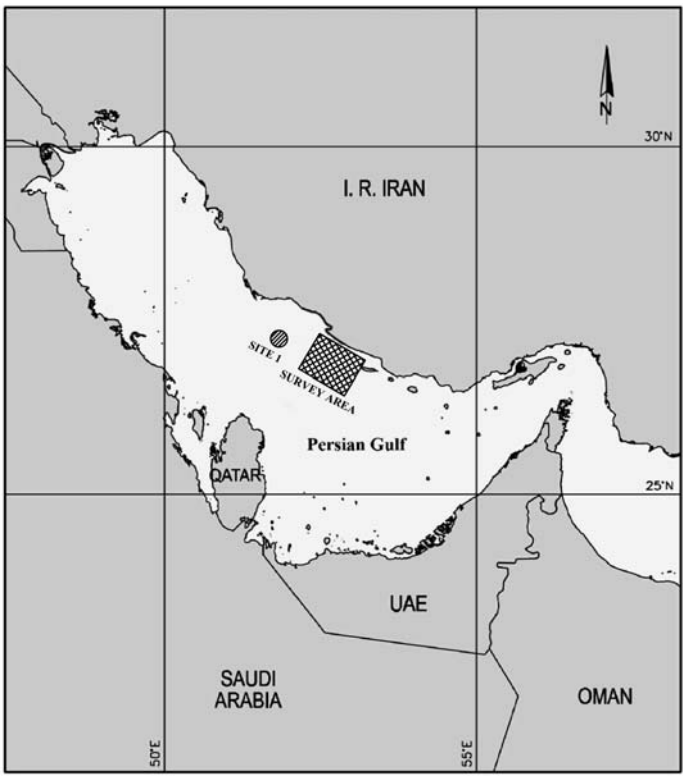

Figure 2. Location of survey area in South Pars Field, south-west of Iran.

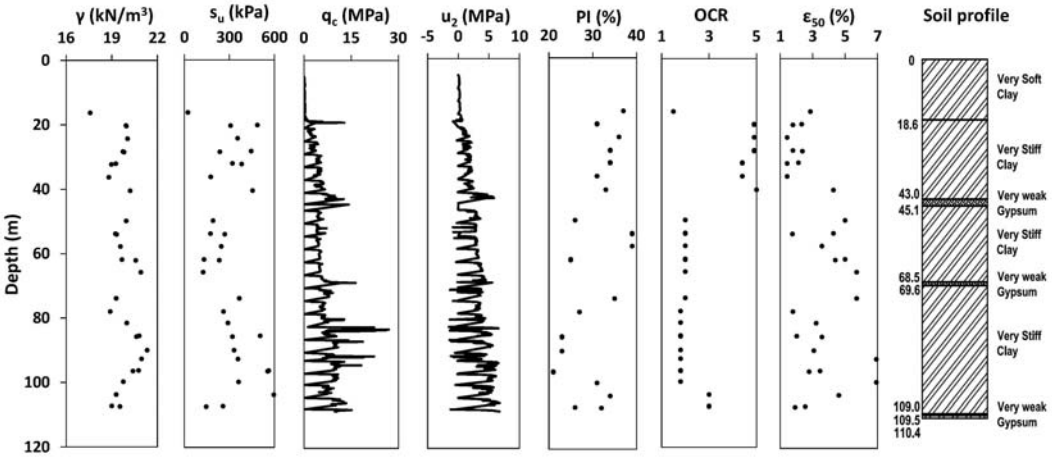

Figure 3. Soil profile and the field and laboratory results for a typical 110 m borehole within survey area.

soil investigation activities were comprised of sixteen boreholes: eight boreholes with a depth of 110 m and the rest with a depth of 80 m below the seabed. In-situ and laboratory tests were carried out to determine the geotechnical properties of the sub-seabed soils. The in-situ tests included piezocone penetration and torvane. Laboratory tests such as unconsolidated undrained (UU) triaxial compression were performed, which resulted in the undrained shear strength of the soil. The strain at 50% of the maximum deviatoric stress (ε_{50}) and the strain at failure were also obtained from stress-strain curves in the UU tests. Atterberg limits and sieve tests were performed as well. Typical profiles of the soil properties are shown in Fig. 3 for a 110 m borehole within the considered survey area. The sub-seabed soils are generally clay, including very soft clay at the top, up to approximately 20 m, which become stiffer with depth. In addition, lenses of sandy silt and gypsum are found at several depths.

3 EVOLUTIONARY POLYNOMIAL REGRESSION

Evolutionary polynomial regression (EPR) is a useful toolbox developed on a modeling methodology based on the hybrid regression method by Giustolisi et al. [15] and Giustolisi and Savic [16]. It is a symbolic data-driven method that is used to create polynomial models to evolutionary compute based on input data and belongs to the family of Genetic Programming [17]. The constitutive modeling of soil [18] and an assessment of earthquake-induced soil liquefaction and lateral displacement [19] are some successful examples of the use of EPR in the field of geotechnical engineering.

The EPR method includes two general stages: searching the model structures based on an integer Genetic Algorithm (GA) and evaluating each of the model parameters, such as the numerical constant coefficients considering linear optimization [16]. The general symbolic expression derived from EPR is as follows:

$$\hat{Y} = \sum_{j=1}^{m} F(\mathrm{X}, f(\mathrm{X}), a_j) + a_0 \qquad (2)$$

where $\hat{Y}$ is the estimated outputs of the system derived from EPR, F is the function constructed by the program, X is the input variables matrix, f is a user-defined function, a_j is an adjustable parameter determined by the program, and m is the number of terms of the expression defined by the user, excluding the bias a_0 , if any. The general process can be rewritten based on vector form as

$$Y_{N\times 1}(\theta, Z) = \left[I_{N\times 1}\ Z^{j}_{N\times n}\right] \times \left[a_0\ a_1 \ldots a_n\right]^{T} = Z_{N\times d} \times \theta^{T}_{d\times 1} \quad (3)$$

where $Y_{N\times 1}(\theta,Z)$ is the least-squares estimate vector of the N target values, $\theta_{d\times 1}$ is the vector of $d = m + 1$ parameters a_j and a_0 (θ^T is the transposed vector), $Z_{N\times d}$ is a matrix formed by I, unitary vector for bias a_0 , and m vectors of variables Z^j that for a fixed j are a product of the independent predictor vectors of inputs, $X = \left\langle X_1 X_2 \ldots X_k \right\rangle$.

The EPR performs an evolutionary search of the model space using an analogy with stepwise regression [20], rather than by means of the traditional symbolic regression search based on parse tree structures. In this way, the EPR performs a global search of the input exponents and a combination of input variables according to the user-defined cost function.

The program search is based on pseudo-polynomial and true structures using a single and multi-objective genetic algorithm, with different general expression forms. The expression form considered in this research is defined as below:

$$Y = a_0 + \sum_{j=1}^{m} a_j . (X_1)^{ES(j,1)} . \cdots . (X_k)^{ES(j,k)} . f\left((X_1)^{ES(j,k+1)}\right) . \cdots . f\left((X_k)^{ES(j,2k)}\right) \quad (4)$$

In the above expression, X_i are the k candidate inputs vectors, a_j are constant values, ES is the matrix of unknown exponents that can be edited by the user within the defined range of values, and m is the length of the expressions defined by the user, which represents the number of maximum terms in each set of results. Each monomial of the polynomial models can contain user-defined functions. For this purpose, $f()$ is the function that can be selected by the user based on available functions in the program. These functions may be logarithmic, exponential, tangent hyperbolic, etc.

In order to determine all the models corresponding to the optimal trade-off between the fitness and the brevity of the model, the EPR performs a multi-objective search exhibiting various mathematical models representing the best fitness for possible models. For a particular purpose, one can choose the best models based on short gap reconstruction, gaining a physical insight or forecasting the phenomenon. The fitness model defined in the EPR is the Coefficient of Determination (CoD), which refers to how closely the regression expression fits the data points:

$$CoD = 1 - \frac{\sum_{n} (p - m)^2}{\sum_{n} (m - \bar{m})^2} \quad (5)$$

where p is the predicted values by model derived from the EPR, m is the measured value, $\bar{m}$ is the average of the measured values, and n is the number of data points. More details about the EPR architecture for model representation as well as the method employed for the parameter estimation can be found in Giustolisi and Savic [16].

4 RESULTS AND DISCUSSION

The field and laboratory test results, including 274 data series, are considered as the databank for the numerical regression. In the present study, five variables are identified as the primary input data of cohesive soils for evaluating ε_{50} as an output. The input data includes the undrained shear strength (s_u), the normalized cone tip resistance (q_c), the total over-burden pressure (σ_0), the plasticity index (PI) and the over-consolidation ratio (OCR).

In pattern recognition procedures it is common practice to divide the available data into two subsets: training and testing. The model is firstly developed using the former and then tested using the latter one to ensure that the final obtained model has the ability to properly estimate ε_{50} for unseen or untrained cases. Here, the entire databank is divided into several random combinations of training and testing sets until a robust representation of the whole population, in terms of statistical properties, is achieved for both training and testing sets. The statistical properties of the parameters considered in this study, including the values of maximum, minimum, mean, and the standard deviation, are presented in Table 1 for the training, testing and all datasets. The training dataset includes 80% of all the data (219), and the rest (55) are used as the testing dataset. The statistical values of the training, testing and all datasets, shown in Table 1, are close to each other.

Table 1. Statistical characteristics of databank.

Subsets	Statistical characteristics	σ_0 (kPa)	s_u (kPa)	q_c (kPa)	PI (%)	OCR	Measured ε_{50} (%)
Testing data (55 data)	Minimum	216	19	162	14	0.9	0.9
	Maximum	1933	504	8767	40	4	9.2
	Mean	1081	241	4155	29	2.2	3.9
	Standard deviation	462	112	2190	6.8	0.74	2.1
Training data (219 data)	Minimum	217	19	139	12	0.9	0.7
	Maximum	2207	634	8943	47	5.3	9.3
	Mean	1077	274	4184	30	2.4	3.5
	Standard deviation	515	129	1996	7.4	1.1	2.0
All data (274 data)	Minimum	216	19	139	12	0.9	0.7
	Maximum	2207	634	8943	47	5.3	9.3
	Mean	1078	268	4178	30	2.4	3.6
	Standard deviation	505	126	2037	7.3	1.0	2.1

Table 2. Proposed models for estimating ε_{50}.

No.	Equation	Involved parameters	R^2 (%)	*RMSE*	*MAE*
Model 1	$\varepsilon_{50} = -0.79 + 1.5 s_u^{0.2}$	s_u	6.6	1.99	1.65
Model 2	$\varepsilon_{50} = 1.48 + 1.2\times10^{-3} q_c^{0.9}$	q_c	20.8	1.84	1.52
Model 3	$\varepsilon_{50} = 4.84 - 8.76\times10^{-2} q_c^{0.3} PI^{0.5} OCR^{-0.1} - 1.24\times10^{-12} q_c^{3.3} OCR^{-0.3} + 5.43\times10^{-6} q_c^{1.4} PI^{0.7} OCR^{-0.1} - 2.1\times10^{-3} q_c^{0.5} PI^{0.8} OCR^{0.7}$	q_c, *PI*, *OCR*	36.7	1.64	1.34
Model 4	$\varepsilon_{50} = 1.55 - 2.7\times10^{-13} \sigma^{1.5} q_c^{2.6} PI^{-1.3} OCR^{-0.2} - 1.8\times10^{-10} \sigma^{0.6} q_c^{1.3} PI^{1.6} OCR^{2} + 1.5\times10^{-6} \sigma^{1.5} q_c^{0.4} PI^{0.1} OCR^{0.6}$	σ_0, q_c, *PI*, *OCR*	64.8	1.22	1.02

After several analyses in the EPR framework, four relationships are developed for evaluating ε_{50} , which are presented in Table 2. To examine the robustness and assess the performance of the EPR models, the following three statistical criteria were used:

- Coefficient of determination (R^2), is a measure used to determine the relative correlation between two sets of variables, and defined as:

$$R^2 = 1 - \frac{\sum_{i=1}^{n}(m_i - p_i)^2}{\sum_{i=1}^{n}(m_i - \overline{m})^2} \qquad (6)$$

- Root mean square error (*RMSE*), is a measure of the error, defined as:

$$RMSE = \sqrt{\frac{\sum_{i=1}^{n}(m_i - p_i)^2}{n}} \qquad (7)$$

The advantage of this criterion is that large errors receive greater attention than smaller ones.

- Mean absolute error (*MAE*) is another measure of the error which eliminates the emphasis given to large errors, presented as:

$$MAE = \frac{\sum_{i=1}^{n}|m_i - p_i|}{n} \qquad (8)$$

In the above relations, m_i and p_i are the i^{th} measured and predicted values of the output parameter (ε_{50}), respectively, n is the number of data points, and $\bar{m}$ indicates the average of the measured output.

The suggested models to evaluate ε_{50} as well as the values of the statistical criteria are presented in Table 2. It is clear that the performance of the models improves from model 1 to 4, since the R^2 value increases while the *RMSE* and *MAE* values decrease. Based on the results summarized in Table 2, the EPR model 4 was chosen as the most appropriate one, which is developed using four input parameters: q_c , σ_0 , *PI*, *OCR* .

The first relationship is developed between the undrained shear strength of the soil and ε_{50} , and the second one uses the normalized cone tip resistance (q_c) to predict ε_{50} , as shown in Table 2. By comparing the statistical characteristics of models 1 and 2, it can be seen that the ε_{50} values predicted from the field-based resistance property (q_c) are more accurate than those predicted from the laboratory-based resistance (s_u). By using q_c instead of s_u , R^2 increases from 6.6 for model 1 to 20.8 for model 2. However, the R^2 value is not yet acceptable, and it seems that other influential parameters should be included in the model development process. Therefore, after several trial-and-error procedures it was found that the index properties of the soil, e.g., *OCR* and *PI*, have strong effects on the predicted ε_{50} values. According to Table 1, it is realized that model 3, which includes the above-mentioned factors, predicts ε_{50} more accurately than model 2. Furthermore, model 4 shows that the over-burden pressure also has a significant positive influence on the prediction accuracy.

Fig. 4 illustrates the predicting capability of the models by plotting the ε_{50} values against their corresponding measured values in training and testing datasets and their statistical characteristics are shown for a quantitative comparison. Considering the data scatter in the graphs of Fig. 4, the results of the models for the testing dataset are generally consistent with those for the

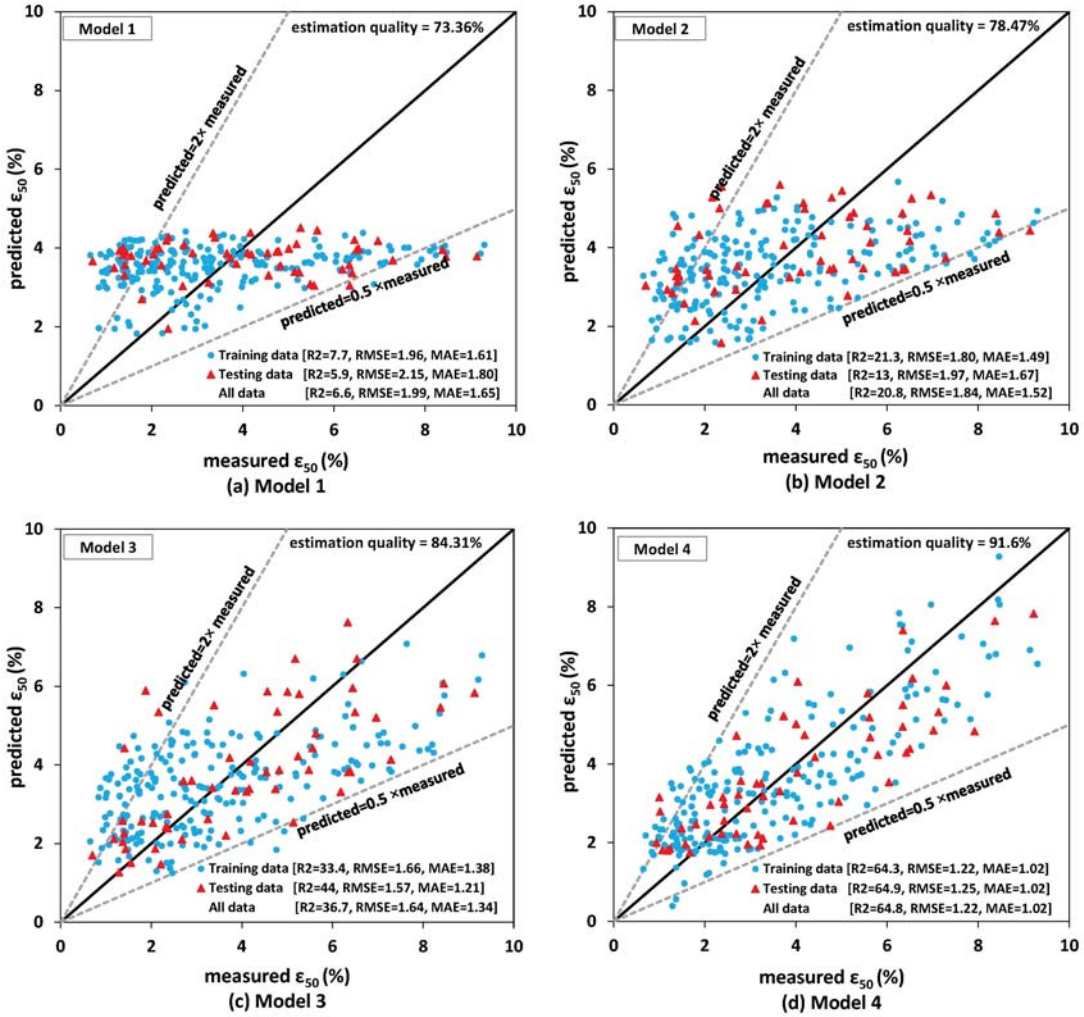

Figure 4. Predicted versus measured ε_{50} values for the proposed EPR-based models.

training dataset. The more the points are distributed uniformly around the ideal 45° line, and the less scatter around this line, the better the capability of the model at predicting ε_{50} . In this regard, it is clear that model 4 behaves better than the others. The upper and lower lines in Fig. 4 show the boundaries for a zone that is characterized by the ratios of the predicted-to-measured ε_{50} between 0.5 and 2.0. The estimation quality of each model, defined as the number of points that fall inside these two boundaries as a percentage of the total points, is shown in the figure. As the performance of the models improves, the data show more concentration in the mentioned zone. While all the models show acceptable estimation qualities, the estimation quality for model 4 has the highest value (91.6%) among the proposed models.

It is clear from Fig 4 that the predicted ε_{50} values from model 1, which was developed merely from the undrained shear strength (S_u), are not well distributed along the diagonal line and are concentrated in a narrow horizontal band. However, implementing the normalized cone tip resistance (q_c), instead of S_u , in model 2 smoothed the above-mentioned shortcoming.

The log-normal distribution, used by Briaud and Tucker [21], is an appropriate statistical criterion to further evaluate the performance of the proposed models. In this regard, the natural logarithm of the ratio of the predicted-to-measured ε_{50} i.e., $\ln(\varepsilon_{50_p} / \varepsilon_{50_m})$, is calculated for each data point and then the mean and standard deviation of these values are determined as follows:

$$\mu_{\ln(\varepsilon_{50p}/\varepsilon_{50m})} = \frac{1}{n}\sum_{i=1}^{n} \ln(\varepsilon_{50p} / \varepsilon_{50m})_i \qquad (9)$$

$$\sigma_{\ln(\varepsilon_{50p}/\varepsilon_{50m})} = \sqrt{\frac{1}{n-1}\sum_{i=1}^{n}\left(\ln(\varepsilon_{50p} / \varepsilon_{50m})_i - \mu_{\ln(\varepsilon_{50p}/\varepsilon_{50m})}\right)^2} \qquad (10)$$

where the subscripts p and m denote the "predicted" and "measured", respectively, n is the number of data considered in the analysis, $\mu_{\ln}$ and $\sigma_{\ln}$ are indicators for the accuracy and precision of the models, respectively, which are used to identify the log-normal distribution of the density function as:

$$f(\varepsilon_{50p} / \varepsilon_{50m}) = \frac{1}{\sqrt{2\pi}\sigma_{\ln}(\varepsilon_{50p} / \varepsilon_{50m})} \exp\left[-\frac{1}{2}\left(\frac{\ln(\varepsilon_{50p} / \varepsilon_{50m}) - \mu_{\ln(\varepsilon_{50p}/\varepsilon_{50m})}}{\sigma_{\ln(\varepsilon_{50p}/\varepsilon_{50m})}} \right)^2 \right] \qquad (11)$$

A better distribution is achieved when $\mu_{\ln(\varepsilon_{50p}/\varepsilon_{50m})}$ and $\sigma_{\ln(\varepsilon_{50p}/\varepsilon_{50m})}$ approach unity and zero, respectively. The log-normal distribution of $\varepsilon_{50p}/\varepsilon_{50m}$ for the proposed models are presented in Fig. 5.

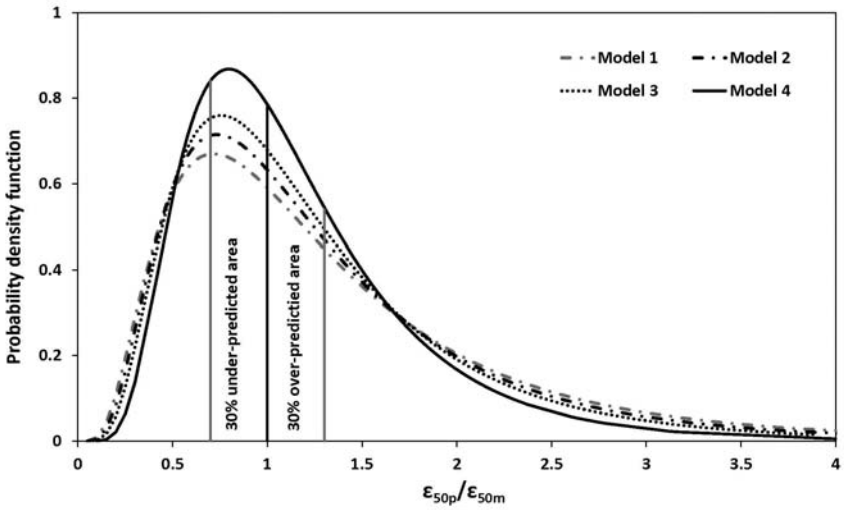

Figure 5. Log-normal distribution of $\varepsilon_{50p}/\varepsilon_{50m}$ for the proposed models.

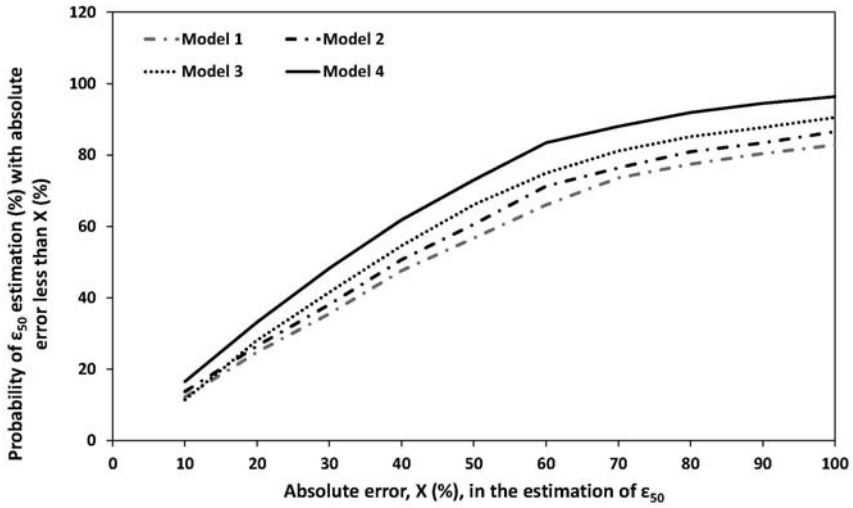

Figure 6. Probability of ε_{50} estimation with absolute error less than a given error, x (%).

The probability of predicting ε_{50} with a 0 to 90% accuracy (10-100% absolute error) is calculated from Fig. 5 and shown in Fig. 6. The total area below each curve in Fig. 5 is equal to one. Therefore, at a specified absolute error level, the probability of predicting ε_{50} is derived by calculating the total area below the log-normal distribution curve within the accuracy limits. At a constant absolute error, a higher probability indicates the better ability of the model at predicting ε_{50} . Based on this definition, the performance of the models improves from model 1 to 4 at all levels of absolute error.

The ability of the different models to predict ε_{50} can be evaluated using cumulative probability, as used by Long and Wysockey [22]. They used the concept of cumulative probability as a criterion to evaluate the bias of their model. The cumulative probability for each $\varepsilon_{50p}/\varepsilon_{50m}$ can be obtained with the following definition:

$$CP_i = \frac{i}{n+1} \qquad (12)$$

where i is the data number arranged in an ascending order. The cumulative probability versus the ratio $\varepsilon_{50p}/\varepsilon_{50m}$ for the proposed models is depicted in Fig. 7. In order to assess the ability of each model at estimating ε_{50}, the 50% and 90% cumulative probabilities (CP50% and CP90%) are calculated. The difference between CP90 and CP50 (CP90%–CP50%) represents the discrepancy from an accurate estimation. Ideally, if all the data are predicted with no bias, the distribution of the estimated-to-measured ε_{50} against CP will be a straight line with a value of unity, indicating an exact estimation. In reality, the better performance of the model is achieved when $\varepsilon_{50p}/\varepsilon_{50m}$ is closer to unity at CP50%. Lower (CP90%–CP50%) for each model indicates the better prediction accuracy of the proposed model. According to this criterion, it is observed in Fig. 7 that model 4 leads to an optimum value of CP50% equal to unity and a lower value of (CP90%–CP50%) compared with the other models.

In a statistical analysis a model would behave better if the residual values, i.e., the difference between the measured and predicted values of ε_{50} , are concentrated more uniformly around the mean value of the residuals. The mean value of the residuals is calculated by:

$$MR = \frac{1}{n}\sum_{i=1}^{n}(\varepsilon_{50m} - \varepsilon_{50p})_i \qquad (13)$$

Fig. 8 (see next page) depicts the residuals of the training and testing sets for all the presented models versus the data number. In this figure, the residuals are scattered along a line indicating the mean (MR). In addition, the upper and lower bounds of the residual scatter ($MR\pm\sigma$; σ is the standard deviation of residuals) are shown in the figure. The ideal performance of each model is achieved by MR and σ equal to zero. In general, the lower absolute values of these two parameters represent the better performance of the model. A comparison between the proposed models in Fig. 8, with respect to the above parameters, shows an improvement of the models from 1 to 4 by decreasing the absolute MR and σ values.

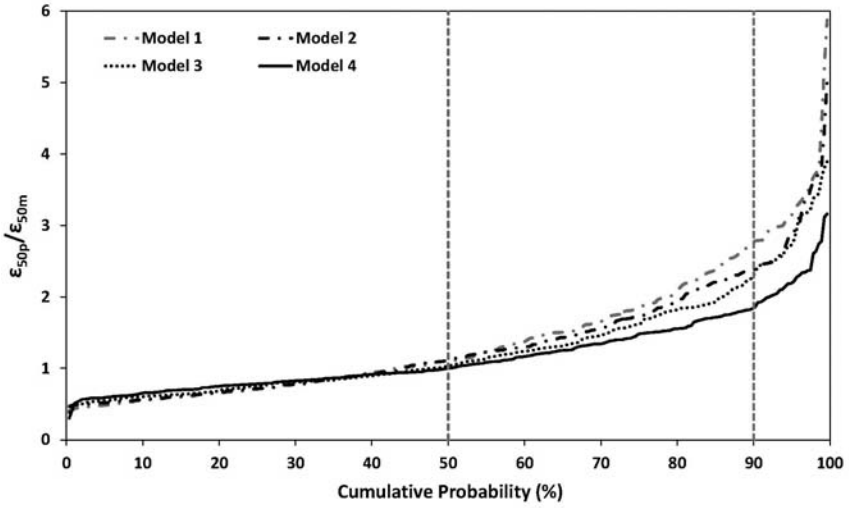

Figure 7. Cumulative probability plot of $\varepsilon_{50p}/\varepsilon_{50m}$ for the proposed models.

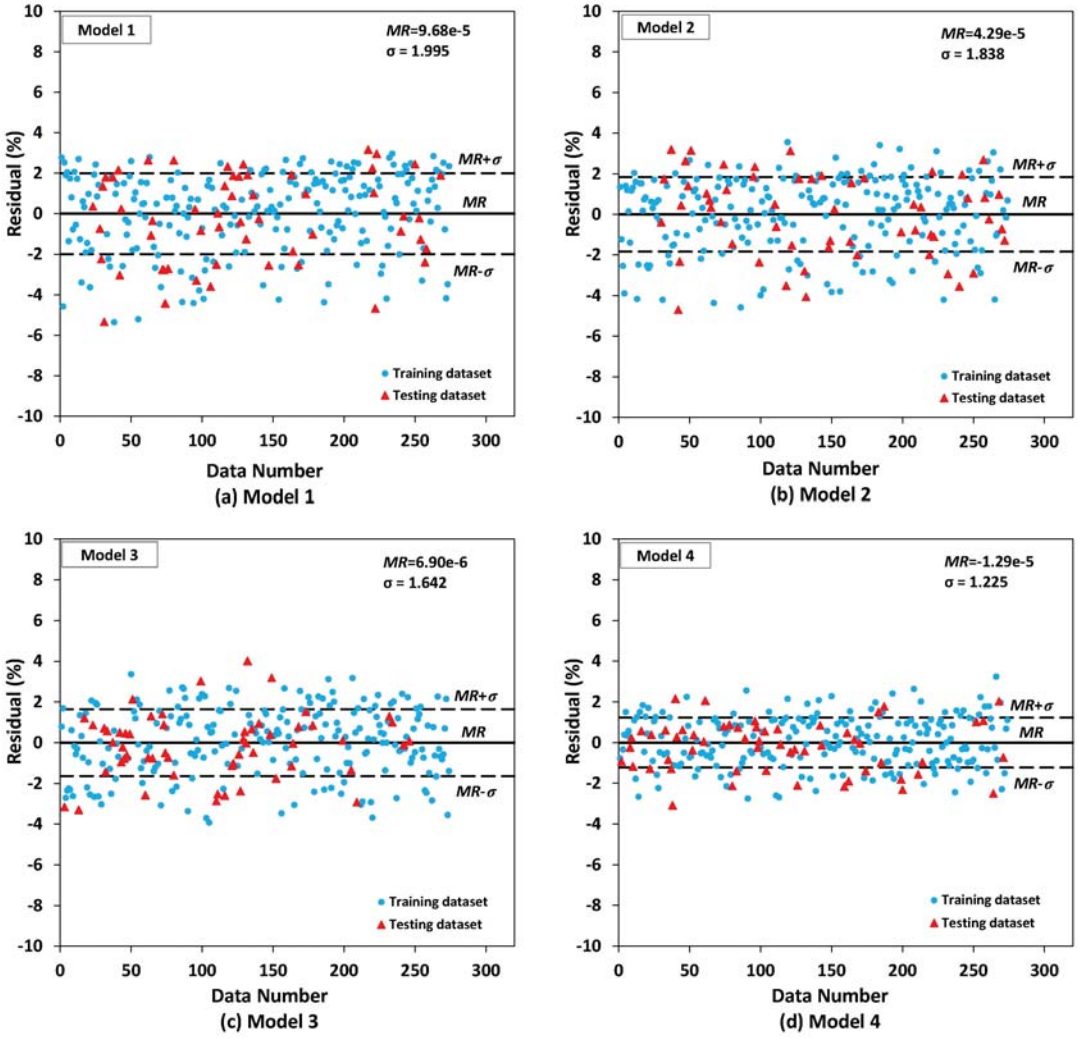

Figure 8. Distribution of residual for the EPR-based models.

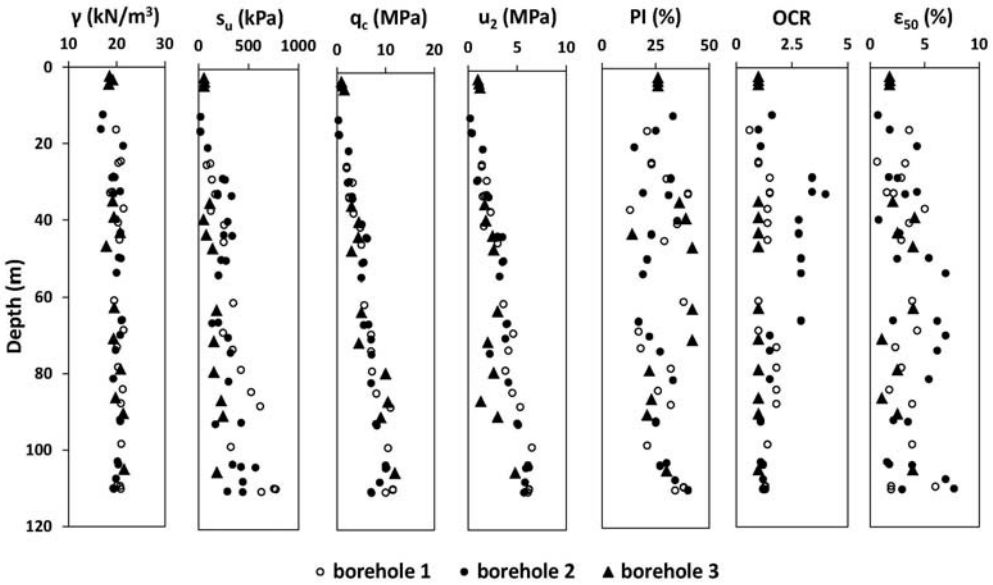

Figure 9. Geotechnical characteristics of soil in the boreholes of Site 1.

5 VALIDATION OF THE PROPOSED MODELS

In order to validate the proposed models, the test results at three different sites are considered. The first site is located at South Pars field, Persian Gulf, Iran, outside the survey area, shown as Site 1 in Fig. 2. The soil is a very soft clay overlying a sandy silt or silty sand layer at shallow depths. Stiff to very stiff clay dominates at deeper parts. The profiles of the soil properties in three boreholes within this site are presented in Fig.9. Fig. 10 shows the ε_{50} values predicted by different models as well as the measured values obtained from UU tests in borehole depths. In all the figures the recommended ε_{50} values by Sullivan et al. [8] are significantly lower than the measured ones. However, the ε_{50} values predicted by models 1 and 4 compare relatively well with the measured ones in the full range of values along the borehole depths, as shown in Fig. 10. Generally, the ε_{50} values show an increasing trend with depth from both laboratory measurements and the predictions of the currently proposed models. This result is in contradiction with the values of ε_{50} recommended by Sullivan.

Herein, it is attempted to validate the current models using the p-y curve results obtained from the pile load tests conducted at two different sites (Sites 2 and 3). General information about the considered sites is given in Table 3.

Figs. 11(a) and (b) show the p-y curves generated based on the ε_{50} values from different models as well as Sullivan's recommendations for two different depths at Sites 2 and 3, respectively. The figures also include the p-y curves obtained from full-scale tests. It is noted that the procedure for generating p-y curves is based on API [27]. The figures show that the calculated p-y curves from the EPR-based models agree relatively well with the measured p-y curves. However, the p-y curves calculated from the Sullivan's recommendations show lower values of the lateral displacement at all the lateral load levels. This implies that using the ε_{50} parameter from the Sullivan recommendations in generating the p-y curve leads to a stiffer behavior of the pile-soil system against lateral loads in comparison with the real behavior. It is observed that the predicted lateral displacements at 50% of the maximum lateral load from the proposed models are 1.5–3.5 and 2–4 times as large as those obtained from the Sullivan recommendations for Sites 2 and 3, respectively.

In addition, the ratio of the predicted-to-measured lateral pile displacements at the maximum lateral load levels for the generated p-y curves at both sites is summarized in Table 6. It is clear from Table 6 that the generated p-y curves based on the ε_{50} values from the proposed models yield lateral pile displacements very close to the measured ones, with a maximum error of 6%. However, using the ε_{50} values from Sullivan's recommendation in generating the p-y curves leads to very non-conservative lateral pile displacements at both sites.

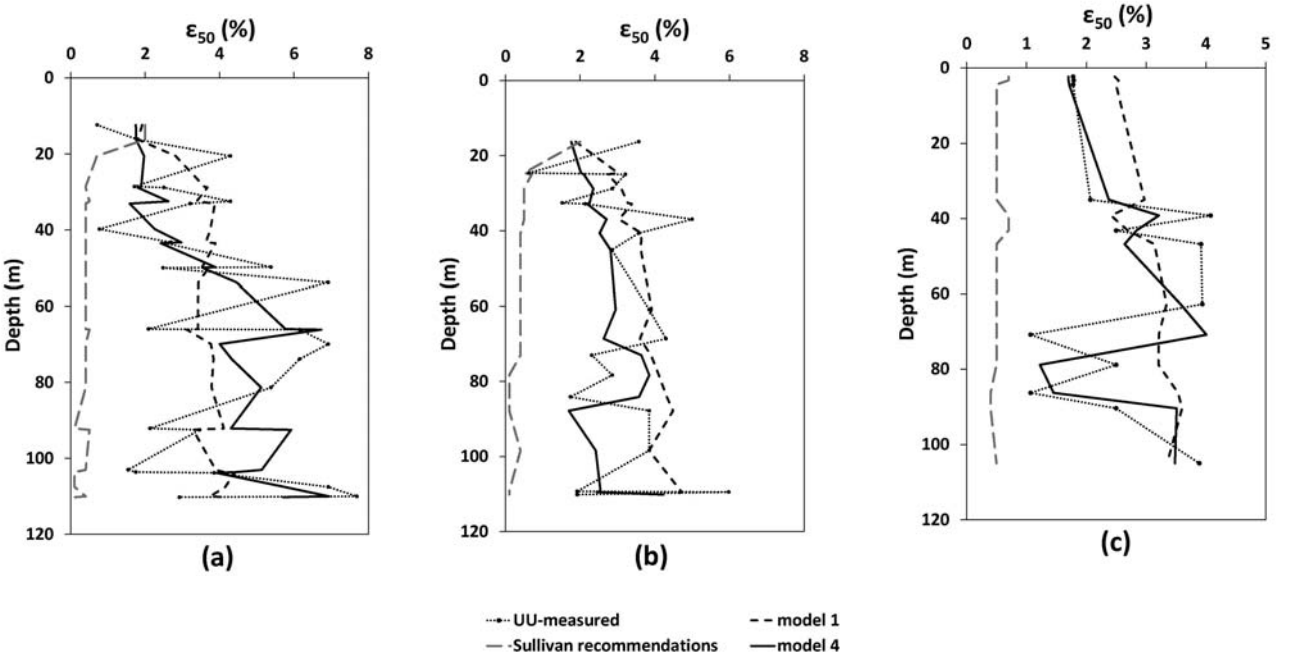

Figure 10. Profiles of predicted and measured ε_{50} values in Site 1 from (a) borehole 1, (b) borehole 2, and (c) borehole 3.

Table 3. General information about Sites 2 and 3.

Site No.	Location	Source of p-y curve data	Pile section	Pile section dimension (m)	Depth of measurement (m)	Pile length (m)	Relevant geotechnical properties	Reference
2	Incheon Bridge, Korea	Full-scale field load tests on piles	Circular	Diameter = 1.016 Thickness= 0.016	4D from ground surface (D= pile diameter)	26.6	Table 4	[23-25]
3	Bridge construction site near Oskaloosa, Iowa	Lateral load tests on steel and concrete piles	UHPC[1] H-shaped	0.254×0.254	5D from ground surface (D=equivalent diameter, 0.287)	10.7	Table 4	[26]

[1] Ultra-high-performance concrete

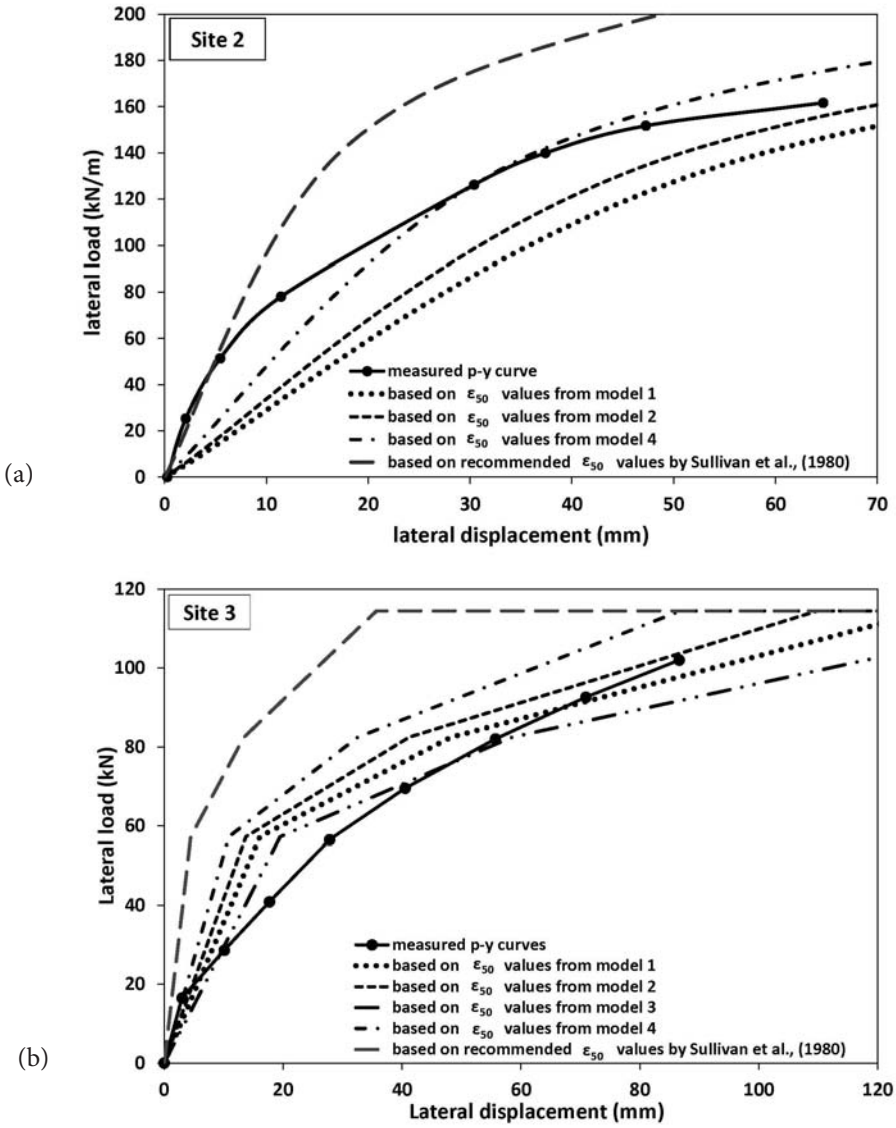

Figure 11. Measured and calculated p-y curves: (a) Site 2 at depth = 4D; and (b) Site 3 at depth = 5D, (D = pile diameter).

Table 4. Soil properties of Site 2 [23-25].

Type	Depth (m)	Unit weight (kN/m^3)	Moisture content (%)	s_u (kPa)	Friction angle (φ) (°)	Recommended ε_{50} in the literature
Upper clay	0-6.3	17.5	21.2	15-30	-	0.02
Lower clay	6.3-16.5	17.5	7.6	30-50	-	0.01
Silty clay	16.5-22.0	17.8	12.7	70	-	0.005
Residual soil	22.0-24.0	18.0	4.33	-	34	-

Table 5. Soil properties of Site 3 [26].

Depth (m)	classification	Unit weight (kN/m^3)	Moisture content (%)	LL (%)	PI (%)	s_u (kPa)	Friction angle (φ) (°)	Recommended ε_{50} in the literature
0-1.5	ML	18.8	21.2	42.1	10.4	60	-	0.007
1.5-2.8	CL	18.5	7.6	44.4	17.9	60	-	0.007
2.8-4.9	CL	18.5	12.7	27.9	7.4	136	-	0.005
4.9-5.8	SC	20.5	4.33	32.5	17.7	-	41	-
5.8-7.7	CL	20.4	4.83	36.7	19.2	-	35	-
7.7-9.2	SW	20.6	20.6	-	-	-	42	-
9.2-10.5	CL	20.4	-	-	-	800	-	0.004
10.5-12.0	SW	20.4	-	-	-	-	-	-

Table 6. Ratio of predicted-to-measured lateral pile displacement.

Site No.	At maximum lateral load level		
	Depth	Average of proposed models	Sullivan et al. [8]
2	4D	1.05	0.36
3	5D	1.06	0.31

6 SUMMARY AND CONCLUSIONS

In this research, the results of the field and laboratory test data of the South Pars field, Persian Gulf, Iran, are used to develop models for evaluating ε_{50} using the EPR. In this regard the cone tip resistance of the CPT and several parameters of cohesive soils (S_u , σ_0 , *OCR* and *PI*) are considered when developing the models. The conclusions are as follows:

- According to the statistical analyses, the models developed using the cone tip resistance (q_c) yield more accurate ε_{50} values than those developed using the undrained shear strength of the soils (S_u) obtained from the UU tests. In general ε_{50} is more realistically predicted using the field-based, instead of the laboratory-based, resistance of the soil.
- The index properties of the soil, e.g., *OCR* and *PI*, significantly improve the performance of the proposed models in predicting ε_{50}.
- According to the statistical criteria, the models that are developed considering the effect of the over-burden pressure (σ_0) lead to better predicted ε_{50} values.
- The models are validated with the field data of Site 1, located outside the main survey area, as shown in Fig. 2. The predicted ε_{50} values are in relatively good agreement with the measured ones for the full range of values along all the borehole depths in this site. It was found that the predicted ε_{50} values from the proposed models increase with soil depth, which agrees with the laboratory measurements.
- Further model validation with the full-scale lateral pile load test data at two different sites demonstrate the models' capability in providing the ε_{50} parameter to generate p-y curves consistent with the real behavior of a pile-soil system measured in the field. In particular, the results indicate that the p-y curves generated based on the ε_{50} values from the proposed models are in better agreement with the field data

rather than the p-y curves obtained from previously recommended ε_{50} values in the literature.

ACKNOWLEDGEMENT

The first author wants to express his sincere gratitude to the Iran's National Elites Foundation (INEF) for the moral support and encouragement.

REFERENCES

[1] Matlock, H. (1970). Correlations for design of laterally loaded piles in soft clay. *Proc. Offshore Technology Conf.*, H.M. Coyle and R.E. Bartoskewitz, eds., Houston, Texas, pp. 577-594.

[2] Reese, L.C. and Welch, R.C. (1975). Lateral loading of deep foundations in stiff clay. *J. Geotech. Geoenv. Eng.*,Vol. 101, No. 7, pp. 633-49.

[3] Reese, L.C., Cox, W.R. and Koop, F.D. (1975). Field testing and analysis of laterally loaded piles in stiff clay. *Proc. Offshore Technology Conf.*, Houston, Texas, pp. 671-690.

[4] O'Neill, M.W. and Gazioglu, S.M. (1984). Evaluation of p–y relationships in cohesive soils. *Proc. Symp. Analysis and Design of Pile Foundations,* ASCE, 1-5 October, pp. 192–213.

[5] Gabr, M.A. and Borden, R. (1988). Analysis of load deflection response of laterally loaded piers using DMT. *Proc. 1st Int. Symp. Penetration Testing*, Balkema, Rotterdam, The Netherlands, pp. 513-520.

[6] Robertson, P.K., Davies., M.P. and Campanella, R.G. (1989). Design of laterally loaded driven piles using the flat dilatometer. *Geotech. Test. J.*, Vol. 12, No. 1, pp. 30-38.

[7] American Petroleum Institute. (1993). Recommended practice for planning, designing and constructing fixed offshore platforms. API recommended practice RP-2A, Washington, D.C.

[8] Sullivan, W.R., Reese, L.C. and Fenske, C.W. (1980). Unified method for analysis of laterally loaded piles in clay. Numerical Methods in Offshore Piling. ICE, London, pp. 135-146.

[9] Hamilton, J.M. and Dunnavant, T.W. (1993). Analysis of behavior of the Tilbrook Grange lateral test pile. Large-scale pile tests in clay. Edited by J. Clarke, Thomas Telford, London, U.K., pp. 448-461.

[10] Hamilton, J.M., Long, M.M., Clarck, J. and Lambson, M.D. (1993). Cyclic lateral loading of an instrumented pile in overconsolidated clay at Tilbrook Grange. Large-scale pile tests in clay. Edited by J. Clarke, Thomas Telford, London, U.K., pp. 381-403.

[11] Dunnavant, T.W. (1986). Experimental and analytical investigation of the behavior of single piles in overconsolidated clay subjected to cyclic lateral loads. Ph.D. Dissertation, University of Houston, Houston, Texas.

[12] Davies, M.P. (1987). Predicting axially and laterally loaded pile behavior using in-situ testing methods. M.Sc. Thesis, Department of Civil Engineering, The University of British Columbia, Vancouver, B.C. .

[13] Schmertmann, J. (1978). Guidelines for cone penetration test, performance and design. Federal highway administration, Report No. FHWA-TS-78-209, U.S. Department of Transportation, Washington, D.C.

[14] Lunne, T., Robertson, P.K. and Powell, J.J.M. (1997). Cone penetration testing in geotechnical practice. Blackie Academic, EF Spon/Routledge Publication, New York.

[15] Giustolisi, O., Savic, D.A. and Doglioni, A. (2004). Data reconstruction and forecasting by evolutionary polynomial regression. *Proc. 6th Int. Conf. Hydroinformatics*, Singapore, pp. 1245-1252.

[16] Giustolisi, O. and Savic, D.A. (2006). A symbolic data-driven technique based on evolutionary polynomial regression. *J. Hydroinf.*, Vol. 8, No. 3, pp. 207-222.

[17] Koza, J.R. (1992). Genetic programming: on the programming of computers by natural selection. MIT Press, Cambridge, MA. ISBN 0-262-11170-5.

[18] Javadi, A.A. and Rezania, M. (2009). Intelligent finite element method: an evolutionary approach to constitutive modeling. *Adv. Eng. Inf.*, Vol. 23, pp. 442-451.

[19] Rezania, M., Faramarzi, A. and Javadi, A.A. (2011). An evolutionary based approach for assessment of earthquake-induced soil liquefaction and lateral displacement. *Eng. Appl. Artif. Intell.*, Vol. 24, pp. 142-153.

[20] Draper, N.R. and Smith, H. (1998). Applied regression analysis. Third Edition, John Wiley and Sons, NewYork.

[21] Briaud, J.L. and Tucker, L.M. (1988). Measured and predicted axial response of 98 piles. J. Geotech. Eng., Vol. 114, No. 9, pp. 984-1001.

[22] Long, J.H. and Wysockey, M.H. (1999). Accuracy of methods for predicting axial capacity of deep foundations. *Proc. OTRC 99 Conf.*, Analysis, Design, Construction, and Testing of Deep Foundation, ASCE, Geotechnical Special Publication 88, pp. 190-195.

[23] Jeong, S.S., Kim, Y.H., Kim J.H. and Shin, S.H. (2007). Cyclic lateral load tests of offshore large diameter piles of Incheon Bridge in marine clay. *Proc. 17th Int. Offshore and Polar Engineering Conf.*, Lisbon, Portugal, 1-6 July, pp. 1353–1361.

[24] Kim, Y.H., Jeong, S.S. and Won, J.O. (2009). Effect of lateral rigidity of offshore piles using proposed p–y curves in marine clay. *Mar. Georesour. Geotechnol.*, Vol. 27, No. 1, pp. 53–77.

[25] Kim, Y. and Jeong, S. (2011). Analysis of soil resistance on laterally loaded piles based on 3D pile-soil interaction. Comput. Geotech., Vol. 38, pp. 248-257.

[26] Suleiman, M., Vande Voort, Th. and Sritharan, S. (2010). Behavior of driven ultrahigh-performance concrete H-piles subjected to vertical and lateral loadings. *J. Geotech. Geoenv. Eng.*, ASCE, Vol. 136, No. 10, pp. 1403-1413.

[27] American Petroleum Institute. (2000). Recommended practice for planning, designing and constructing fixed offshore platforms-working stress design. API recommended practice RP-2A, 21st edition, Washington, D.C.